5
Improved Rectification Behavior of ZnO Nanorods Homojunction by Suppressing Li Donor Defects Using Li-Ni Co-doping

5. 1 Introduction

1-D ZnO nanostructures has attracted attention of research community among number of other compound semiconductors due to its unique physical properties e.g. direct and wide band gap, high exciton binding energy, high electron mobility, large piezoelectricity and low thermal expansion. These properties allow ZnO to have higher luminous efficiency and make it a suitable candidate for different semiconductor device applications. Apart from that, ZnO is a non-hazardous material implicating environmental safety and both zinc and oxygen are found in abundance in nature ensuring its easy availability. ZnO 1-D nanorods enriched with these properties has been exploited and is implemented in several applications i.e LEDs, FETs, gas sensors, biological sensors, solar cells, memory devices, solar blind UV photodetector and nanogenerators.

ZnO has intrinsic n-type conductivity and have carrier concentration in the range of 10^{16}-10^{19} /cm^3 (Snigurenko et al., 2015). Controlling the conductivity of ZnO is a challenging aspect as a small various in point defects or dopant concentration can change optical, electrical and structural properties. However, obtaining stable p-ZnO is even more challenging as native point defects or unintentional impurity dopants will lead to self-compensation of the introduced acceptors. Apart from that, acceptors introduced also behaves like deep acceptors and few acceptors have low solubility which further limits the number of suitable acceptors to realize p-type ZnO.

Realization of ZnO based optoelectronic devices generally requires a p-n junction diode. The intrinsic presence of donor type defects limits the realization of stable p-type ZnO; hence ZnO bases p-n junction is synthesized with other p-type materials. There are several heterojunction optoelectronic devices which have been reported over the years to achieve high efficiency. For example, heterostructured p-n junction based ZnO diodes such as p-Si/n–ZnO PDs (Wang et al., 2016), Se/n–ZnO PDs (Hu et al., 2016), p-GaN/i–Al_2O_3/n-ZnO LEDs (Yang et al., 2017), p-GaN/n–ZnO LEDs (Yao et al., 2016) are synthesized and studied where complexity of p-type ZnO is omitted by using p-type substrates of other materials. To ensure high optical and electrical outcomes, both p and n-type materials should exhibits same lattice parameters, crystal structures and band alignment. Large lattice mismatch between the material leads to interface defects and states. These defects contribute in generating higher dislocation density which further limits the junction electrical performances, showing low luminance efficiency (Baek et al., 2016). Hence, number of p-type substrates used for ZnO based heterojunction devices is limited. The most explored p-type materials with least lattice mismatch are GaN and SiC which are expensive and put restrictions on the low cost ZnO based optoelectronic devices. Thus, homojunction based ZnO devices offering least lattice mismatch is important to realize in

order to have high luminous efficiency (Baek et al., 2016; Hsu et al., 2017). However, realizing p-type ZnO to achieve homojunction based devices is a challenging aspect.

Several dopants are investigated to synthesize stable p-ZnO over past few years. The p-type dopant should be able to provide high carrier concentration, reasonable mobility and low resistivity. Group-I elements like lithium (Li), sodium (Na), and potassium (K) are substituted on Zn sites (Gupta et al., 2011; Zeng et al., 2006; Zhang et al., 2014), group-V elements like nitrogen (N), phosphorus (P), arsenic (As), and antimony (Sb) are substituted on O sites (Gautam et al., 2009; Hsu et al., 2005; Sun et al., 2007; Yang et al., 2008) and group-XI elements like copper (Cu), silver (Ag), and gold (Au) are doped on Zn sites (Georgekutty et al., 2008; Hongsith et al., 2008; Pan et al., 2010) for the synthesis of p-ZnO semiconductor. Nitrogen is the most widely studied dopant for realization of p-type ZnO apart from that other group V element suffers from stability issue in p-ZnO (C. H. Park et al., 2002). However, lower defect energy level is observed in p-ZnO doped by group I element which resulted in relatively stable p-type ZnO (Cao and Ji, 2018).

Lithium is one such group I element which has ionic radii (0.76 Å) similar to zinc atom (0.74 Å) and thus, is a suitable choice for p-type dopant (Shakti et al., 2018). Lithium atoms substituted at ZnO site acts as shallow acceptor however, owing to its smaller size it can migrate in interstitial position in ZnO lattice. These interstitial lithium atoms act as shallow donor which compensates the effect of acceptor and leads to unstable characteristics of p-ZnO (B. Y. Zhang et al., 2010). Further, it is reported that co-doping of lithium with hydrogen resulted in higher resistivity of the p-ZnO (Senthil Kumar et al., 2011). Hence, it is important to stabilize the p-ZnO by lithium dopants by various co-doping technique. The co-doping method is supposed to enhance the solubility limit of dopant by bringing the energy levels near to shallow regions. Li-Ni co-doped p-ZnO thin film has been reported to show stable p-ZnO characteristics with low resistivity and further thin film based homojunction devices are also reported (Senthil Kumar et al., 2011).

Vacuum based method such as PLD, MBE, CVD and sputtering is widely sued to synthesize p-ZnO. These methods offer high temperature to provide necessary activation energy of dopants but also put limitation on the realization of p-ZnO on flexible substrate and also suffer from high system cost. In contrast, solution methods are economical and require low temperature for ZnO nanostructure synthesis. Apart from that, understanding of nucleation and growth condition further provides the control on the morphology of nanostructures. Hence, synthesis of ZnO nanorods with solution method is essential in order to have economical and simple synthesis of homojunctions.

In this chapter, we address the Li donor compensation of $Zn_{0.98}Li_{0.02}O$ nanorods by co-doping with Li-Ni atoms. We have carried out a comparative study for solution processed n-ZnO/p-$Zn_{0.98}Li_{0.02}O$ and n-ZnO/ p-$Zn_{0.96}Li_{0.02}Ni_{0.02}O$ nanorods based homojunctions. Li-Ni co-doped p-ZnO based thin film homojunction is reported by Kumar et al. (E. Senthil Kumar et al., 2011), however no reports are available on nanorods based homojunction.

5. 2 Experiments

We have first synthesized pristine n-ZnO, p-$Zn_{0.98}Li_{0.02}O$ and p-$Zn_{0.96}Li_{0.02}Ni_{0.02}O$ nanorods for comparative studies of p-ZnO and n-ZnO thin films. Further, homojunctions are fabricated by realizing n-type ZnO over doped p-type ZnO nanorods for further studies. Two step solution processes is adopted to realize all the samples on n-type silicon substrate (111). Silicon substrates are subjected to the RAC-1& RAC-2 cleaning process prior to synthesizing

nanorods. Since n-Si and ZnO has higher lattice mismatch, hence a seed layer of n-ZnO is deposited before synthesising nanorods.

5.2.1 Seed Layer Deposition

ZnO seed layer is synthesized on cleaned silicon substrate by using sol-gel method. The solution is formulated by dissolving 10 mM of zinc acetate dihydrate ($Zn(O_2CCH_3)_2(H_2O)_2$) and 10mM of monoethanolamine (MEA) in 20 ml of isopropyl alcohol (IPA). The solution is mechanically stirred at room temperature for 2 hours to obtain homogeneous gel and then it is left for ageing at room temperature for 24 hours prior to spin coating. The seed layer is spin coated on silicon for 30 seconds at 3000 rpm. The coated samples are preheated at hot plate in air at 300°C for 2 minutes to ensure dissociation of the salts. This spin coating and preheating process is repeated 5 times to obtained seed layer of thickness ~70 nm. Finally, the coated seed layers are heated for 3 hours in open air furnace at 450°C to achieve the desired crystallinity.

5.2.2 Preparation of $Zn_{0.98}Li_{0.02}O$ and $Zn_{0.96}Li_{0.02}Ni_{0.02}O$ Nanorods

Solution to deposit n-ZnO nanorods are prepared by dissolving 25 mM equimolar zinc acetate dihydrate and hexamethylenetetramine ($C_6H_{12}N_4$) (HMTA) in 300 ml of DI water. $Zn_{0.98}Li_{0.02}O$ nanorods are synthesized by using the similar solution with a lithium dopant source. 300 ml of DI water is used to dissolve 25mM equimolar solution of zinc acetate dihydrate and HMTA. To ensure lithium doping, further 2 mol% lithium acetate dihydrate ($C_2H_3LiO_2 \cdot 2H_2O$) is dissolved in the above solution. Similar approach is adopted to synthesize $Zn_{0.96}Li_{0.02}Ni_{0.02}O$ nanorods. Lithium and nickel doping is achieved by dissolving 2 mol% lithium acetate dihydrate and 2 mol% nickel acetate tetrahydrate ($Ni(CH_3CO_2)_2 \cdot 4\,H_2O$) along with zinc acetate and HMTA in another 300 ml DI water. All the solutions are mechanically stirred for one hour at room temperature to achieve a homogenous cloudy solution. After that, the seed layer coated substrates are placed in a Teflon substrate holder such that seeded layer is facing upside down. Further, the solution containing substrates are placed in an oven for 3 hours at 93 °C. After that, samples are taken out and cleansed with DI water many times to remove any loosely attached material and further dried with nitrogen gun. The samples are then finally annealed for 3 hours at 450 °C to get the desired ZnO, $Zn_{0.98}Li_{0.02}O$ and $Zn_{0.96}Li_{0.02}Ni_{0.02}O$ nanorods. To compare the p-type conductivity of these doped ZnO nanorods, a pristine ZnO nanorods sample is also prepared using the same method without any dopant.

5.2.3 Synthesis of Homojunction Structures

ZnO based p-n homojunctions are synthesized by the similar process described above. Initially, p-type $Zn_{0.98}Li_{0.02}O$ and $Zn_{0.96}Li_{0.02}Ni_{0.02}O$ nanorods are synthesized on two different seeded substrates by doping with Li and Li-Ni respectively. The substrates are dipped in respective solutions and are kept in an oven for 90 minutes at 93 °C. After p-type growth, samples are taken out and dried using nitrogen gun. These samples are further kept in n-type solution without any doping and placed into an oven at 93 °C for another 90 minutes. Further, these samples are retrieved and washed with DI water many times to remove any surface residuals. Finally, the samples are dried in a furnace for 3 hours at 450 °C. The schematic of the process is shown in figure 5.1.

5. 3 Results and Discussion

5.3.1 Structural and Microstructural Characterization of Nanorods and Homojunctions

Structural analysis of doped and pristine samples are investigated using a Bruker D8 powder diffraction system with a Cu-Kα X-ray source (λ=0.15418 nm). The scanning of the samples is performed between 10-80° 2θ range. The diffraction patterns of all three samples substantiated the have preferred orientation along (002) plane and hence are highly c-axis

oriented. The preferred orientation along c-axis substantiates highly aligned nanorods synthesis on the samples. All the observed peaks belong to hexagonal wurtzite structure and matched well with ICDD # 36-1451 substantiating pure phase synthesis of nanorods. The XRD patterns of the samples are presented in figure 5.2 (a).

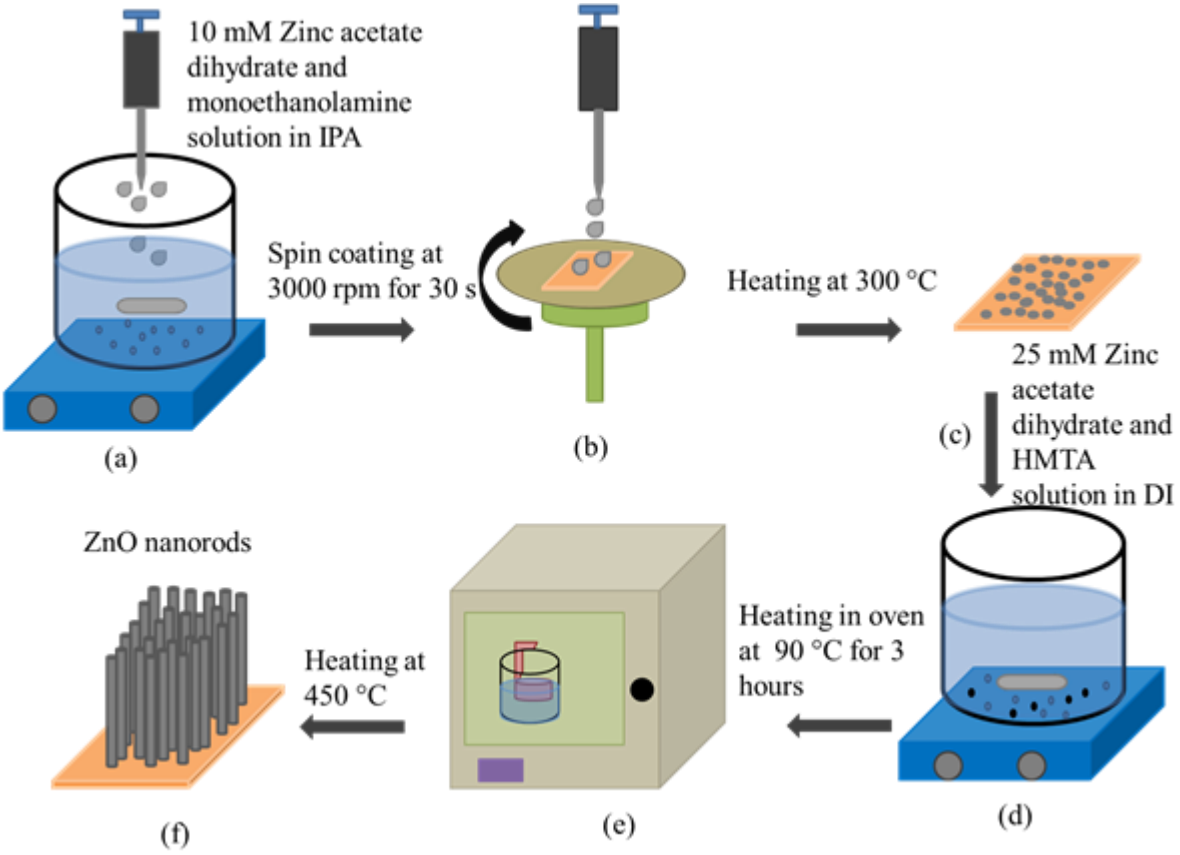

Figure 5.1: Schematic representation of (a) ZnO gel preparation, (b) Spin coating, (c) Drying, (d) Dipping in growth solution, (e) Growth in oven and (f) Synthesized nanorods

Relative shift in 2θ is observed in $Zn_{0.98}Li_{0.02}O$ and $Zn_{0.96}Li_{0.02}Ni_{0.02}O$ samples towards higher side in comparison to pristine ZnO nanorods, Figure 5.2 (b). This shift indicates incorporation of doped atoms inside the ZnO lattice. There is no significant changes in the lattice parameters such as lattice constant, bond length and d spacing, substantiating the uniform substitution of dopant atoms in ZnO crystal (Thakur et al., 2015). However, an increase in crystallite size and slight decrease in strain is observed for doped and co-doped samples with respect to pristine ZnO nanorods. The various estimated parameters of doped and pristine samples are given in Table 5.1.

Table 5.1 : Various Parameters for Doped and Pristine ZnO Nanorods, Estimated from XRD

Sample	FWHM (degree)	2θ (degree)	d (Å)	a (Å)	c (Å)	Crystallite Size (nm)	strain	Bond length (Å)
ZnO	0.404	34.4	2.606	3.19	5.212	21.51	0.326	1.962
$Zn_{0.98}Li_{0.02}O$	0.394	34.42	2.605	3.189	5.209	22.06	0.318	1.952
$Zn_{0.96}Li_{0.02}Ni_{0.02}O$	0.37	34.44	2.603	3.187	5.206	23.49	0.298	1.951

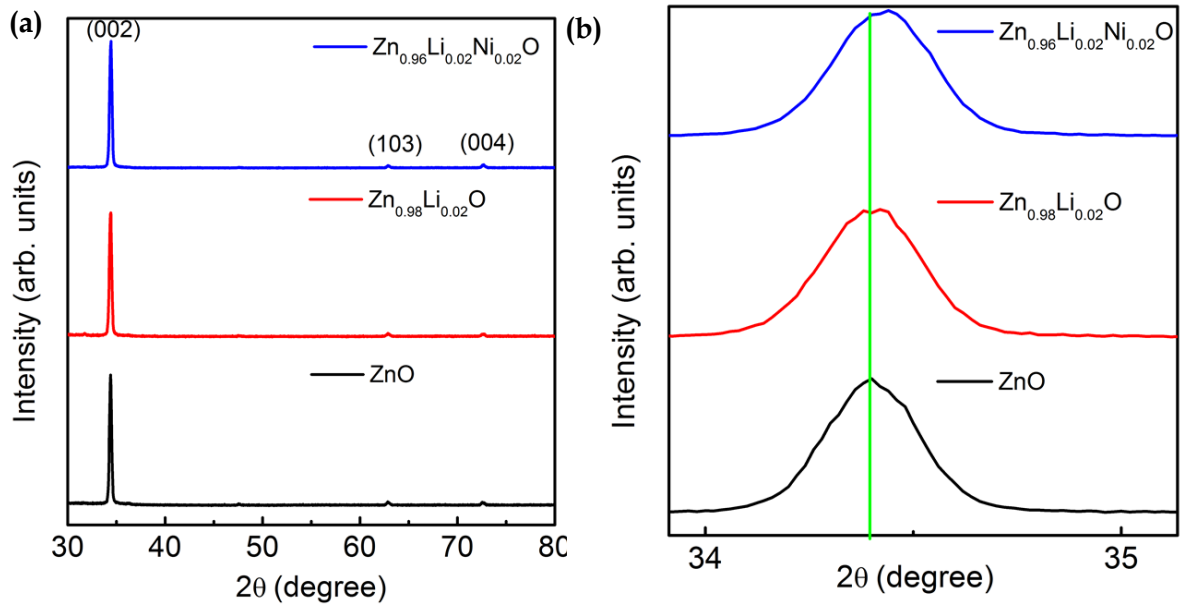

Figure 5.2 : (a) XRD graphs for ZnO, $Zn_{0.98}Li_{0.02}O$ and $Zn_{0.96}Li_{0.02}Ni_{0.02}O$ nanorods on Si substrate and (b) Enlarged view of XRD between 34-35° for identifying any relative shift in (002) diffraction peak

Microstructural and morphological information of the samples are investigated using SEM measurements. Top surface images of ZnO, $Zn_{0.98}Li_{0.02}O$ and $Zn_{0.96}Li_{0.02}Ni_{0.02}O$ nanorods are shown in figure 5.3. All the images substantiate formation of nanorods. The synthesized nanorods are vertically oriented and uniformly distributed throughout the sample. Slight variation in diameter of the nanorods is observed in different samples and the average diameter is ~120±5 nm. The measured heights of all the samples are ~2 µm. Further, to ensure formation of nanorods based homojunctions in these p-n junction samples, cross-sectional SEM measurements are carried out which is shown in the lower part of Figure 5.3, with schematics as an inset in the respective images. The analysis supports vertically aligned and homogenously distributed nanorods junctions. The observed dimeter is ~ 130 nm and height is ~ 2 µm. the realization of n-ZnO nanorods on p-ZnO nanorods are marked by green circles in the cross sectional images.

5.3.2 Optical Characterization

The band gap and optical properties of the pristine and doped samples are analysed by UV-Vis DRS measurements. Graph of absorption coefficient is plotted against wavelength and shown in figure 5.4 (a). It is reported that doping of Ni in ZnO leads to Ni-d band splitting which is attributed to the main source of reduced resistivity in ZnO (S. Singh et al., 2006). The d-band splitting was observed in DRS spectra of Ni-ZnO. Based on that, we assumed that similar effect should be present in case of $Zn_{0.96}Li_{0.02}Ni_{0.02}O$ nanorods. However, we could not observe the Ni band splitting, which should be appearing in the range of 400-700 nm in our $Zn_{0.96}Li_{0.02}Ni_{0.02}O$ nanorods. The presence of thickness fringes in our case might be superimposing on the splitting curve. Further, the band gap of these nanorods are calculated by using Kubelka-Munk model by plotting $(\alpha h\upsilon)^2$ against $h\upsilon$; where h is Plank's constant, α is absorption coefficient and υ is frequency, given in figure 5.4 (b) for all the samples. The estimated bandgap values for pristine ZnO, $Zn_{0.98}Li_{0.02}O$, and $Zn_{0.96}Li_{0.02}Ni_{0.02}O$ nanorods are 3.14 eV, 3.13 eV and 3.12 eV, respectively. The results substantiate that the bandgap of doped ZnO nanorods is decreasing slightly in comparison to pristine ZnO nanorods.

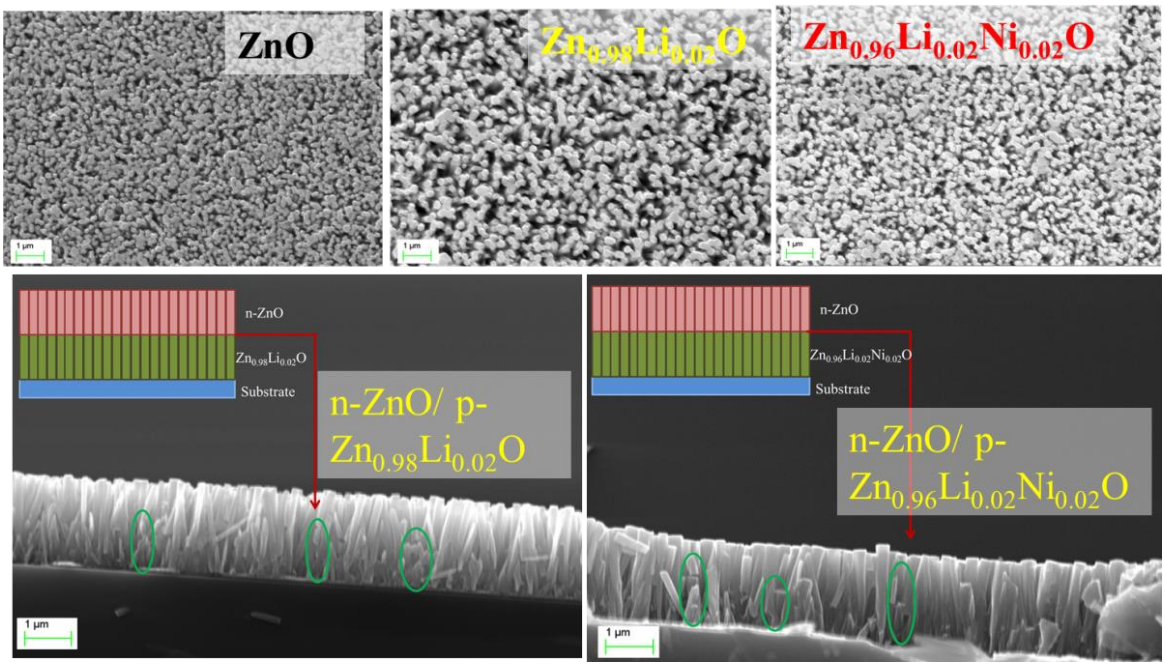

Figure 5.3 : Top surface SEM images of ZnO, $Zn_{0.98}Li_{0.02}O$ and $Zn_{0.96}Li_{0.02}Ni_{0.02}O$ nanorods and cross-sectional images of ZnO/ $Zn_{0.98}Li_{0.02}O$ and ZnO/ $Zn_{0.96}Li_{0.02}Ni_{0.02}O$

To understand the band edge emission ad point defects present in the system, room temperature PL is investigated for all the samples. The measured normalised PL spectrum is shown in the inset of figure 5.4 (a). High intensity, Sharpe and narrow peak is observed for all the sample in Uv range centred at ~~ 378 nm. This peak is attributed to exciton recombination or band to band recombination and is termed near band edge emission (NBE). This peak is positioned at the same point in UV region for all three samples. The calculated band gap is 3.28 eV, slightly greater than the observed band gap from DRS spectra. Another broad peak with varying intensity is observed in 400-700 visible range. The weak emission in green –orange region corresponds to defects level emission (DLE) (Kumari et al., 2018a). The DLE emission is attributed to various intrinsic point defects energy levels inside the doped and undoped ZnO lattice. DLE region have two peaks centered at ~500 nm and ~ 610 nm corresponds to green and orange emission, respectively (Kwon et al., 2018). DLE emission for $Zn_{0.96}Li_{0.02}Ni_{0.02}O$ nanorods, centered at 500 nm is higher in intensity with respect to pristine ZnO and $Zn_{0.98}Li_{0.02}O$ nanorods.

This peak is attributed to zinc interstitials or oxygen vacancies substantiating that point defects present in $Zn_{0.98}Li_{0.02}O$ nanorods are relatively higher than other two samples. These defects acts as shallow donor and compensate the acceptor effect hence, presence of these defects are not favourable. The other peak which is centered at 612 nm is assigned to orange emission and it showed relatively higher intensity for $Zn_{0.96}Li_{0.02}Ni_{0.02}O$ nanorods, substantiating the presence of more zinc and oxygen interstitial atoms (Kwon et al., 2018). The estimated green/UV ratio for ZnO, $Zn_{0.98}Li_{0.02}O$ and $Zn_{0.96}Li_{0.02}Ni_{0.02}O$ is 0.013, 0.025 and 0.068, respectively. the increase ratio from pristine to codoped samples substantiates the incorporation of defect (Hsu et al., 2017).

5.3.3 Electrical Characterization of Homojunctions

To investigate electrical properties, circular silver contacts of 1 mm diameter at 1 mm distance are deposited. Carrier concentrations of the samples are estimated by using Mott-Schottky (M-S) plot. The comparative M-S plots for $Zn_{0.98}Li_{0.02}O$ and $Zn_{0.96}Li_{0.02}Ni_{0.02}O$ nanorods with respect to pristine ZnO nanorods are shown in figure 5.5 (a&b), respectively. carrier concentrations of samples are estimated using the linear slope of M-S plots represented by the

formula, slop = $2/\varepsilon\varepsilon_0 A^2 q N_D$, where q represents charge of the electron, A represents effective electrode area, ε denotes permittivity of the ZnO, ε_0 is the free space permittivity, ND represents donor concentration, and slope is the slope of the linear part of M-S plot (Windisch and Exarhos, 2000).

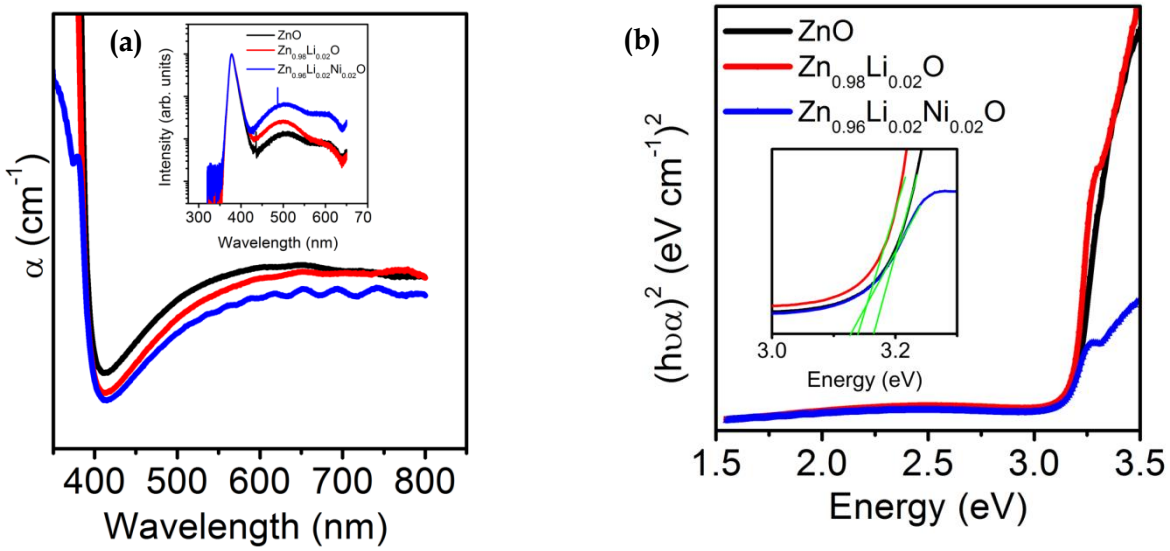

Figure 5.4: (a) DRS absorption data of ZnO, $Zn_{0.98}Li_{0.02}O$ and $Zn_{0.96}Li_{0.02}Ni_{0.02}O$ with PL spectra in the inset and (b) Bandgap of ZnO, $Zn_{0.98}Li_{0.02}O$ and $Zn_{0.96}Li_{0.02}Ni_{0.02}O$ with zoomed region

It is evident from the graph that ZnO has positive slop, representing n-type conductivity and negative slope is observed for $Zn_{0.98}Li_{0.02}O$ and $Zn_{0.96}Li_{0.02}Ni_{0.02}O$, suggesting their p-type nature. The estimated effective carrier concentration for ZnO is $1.17x10^{17}/cm^3$ electrons and for $Zn_{0.98}Li_{0.02}O$ and $Zn_{0.96}Li_{0.02}Ni_{0.02}O$, $1.08x10^{16}$ /cm³ and $1.43x10^{18}$ /cm³ holes, respectively. The results substantiate an increased acceptor concentration in $Zn_{0.96}Li_{0.02}Ni_{0.02}O$. This result supports than the interstitial lithium is acting as a shallow donor in $Zn_{0.98}Li_{0.02}O$, which is reduced in $Zn_{0.96}Li_{0.02}Ni_{0.02}O$ nanorods, and resulting in higher acceptor concentrations. When lithium is doped along with nickel then lithium tends to substitute near nickel. Further, monodoping of Ni transition metal prefers +2 configurations, however, introduction of an acceptor with transition metal favours to have +3 configurations (Senthil Kumar et al., 2011). Hence, introduction of lithium will favour the formation of Ni^{+3} which will act as active donor. This donor will form a complex with Li^+ form Li^+-Ni^{3+}-Li^+ (acceptor-donor-acceptor) complex and is held responsible for p-type conduction (Senthil Kumar et al., 2011). Ni^{+3} will increase the solubility of lithium and will bring the energy level near to shallow region.

After ensuring the formation of p-type $Zn_{0.98}Li_{0.02}O$ and $Zn_{0.96}Li_{0.02}Ni_{0.02}O$ nanorods, I-V measurements are performed on the homojunctions to extract various parameters. I-V measurements are carried out in top n-types surface of $Zn_{0.98}Li_{0.02}O$ and $Zn_{0.96}Li_{0.02}Ni_{0.02}O$ based homojunction samples in between two top contacts to ensure that Schottky contact is not formed between the silver electrode and nanorods. This is shown schematically in the inset of Figure 5.5 (c). The obtained result of this I-V measurement shows that the response is linear, ensuring ohmic contact formation, figure 5.5 (c). Further, to ensure the rectification behaviour of homojunctions, I-V analysis is carried out on Ag/n-ZnO/p-ZnO/Si diode configuration which substantiates rectification behaviour for n-ZnO/ p- $Zn_{0.98}Li_{0.02}O$ and n-ZnO/ p- $Zn_{0.96}Li_{0.02}Ni_{0.02}O$ homojunction, shown in figure 5.5 (d). The rectification ratio (I_{on}/I_{off}) for $Zn_{0.98}Li_{0.02}O$ and $Zn_{0.96}Li_{0.02}Ni_{0.02}O$ based homojunction devices are 204 and 892 at 10 V, respectively.

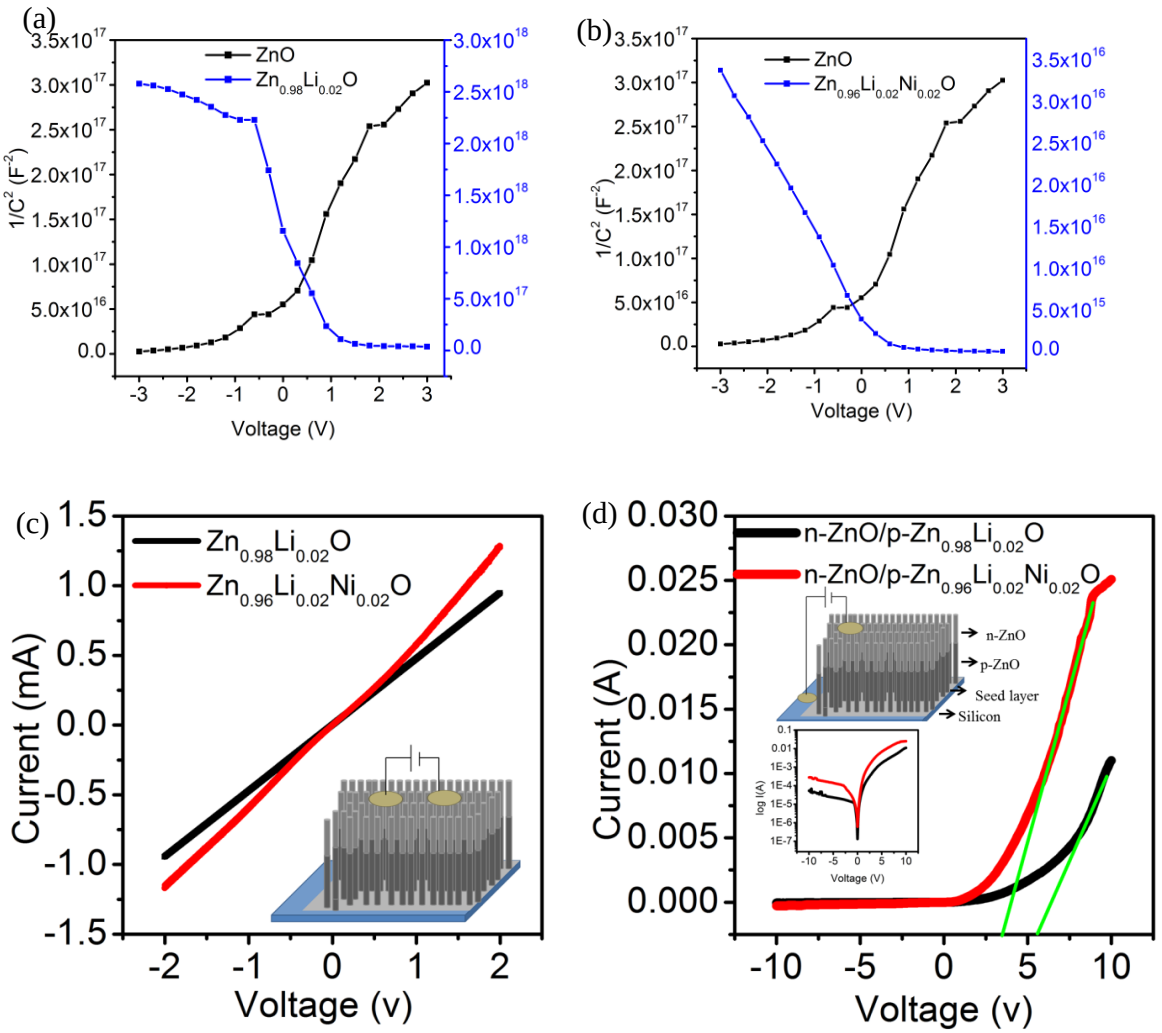

Figure 5.5: Comparative Mott-Schottky plot for (a) $Zn_{0.98}Li_{0.02}O$, (b) $Zn_{0.96}Li_{0.02}Ni_{0.02}O$ with n-ZnO nanorods, (c) n-n contact current voltage characteristics and (d) p-n junction characteristics of $Zn_{0.98}Li_{0.02}O$ and $Zn_{0.96}Li_{0.02}Ni_{0.02}O$ based p-n junction

The estimated turn-on voltage for $Zn_{0.98}Li_{0.02}O$ and $Zn_{0.96}Li_{0.02}Ni_{0.02}O$ based homojunctions are ~5.6 V and ~3.4V, respectively. Hence, it is evident from the results that $Zn_{0.96}Li_{0.02}Ni_{0.02}O$ based homojunction exhibits lower turn on voltage in conjunction with higher rectification ratio in comparison to $Zn_{0.98}Li_{0.02}O$ based homojunction. The higher rectification ratio for $Zn_{0.96}Li_{0.02}Ni_{0.02}O$ homojunction device may be attributed higher acceptor concentrations. Further, ideality factors and barrier heights of homojunction devices are calculated by a thermionic emission model represented by the formula

$$I = I_s[\exp(qV/\eta k_B T)-1], \quad (5.1)$$

where, I represents diode current, I_s is reverse saturation current, q is the electron charge, V is the applied voltage across the device, η is ideality factor, K_B is Boltzmann constant and T is temperature in Kelvin (Somvanshi and Jit, 2014). The semilogrithim I-V curve i.e. ln(I) versus voltage curve is plotted to calculate η in lower voltage region, Figure 5.6 (a) and 5(b) where slope is used to estimate $\eta = q/k_B T\,[dV/d\ln(I)]$ (Vabbina et al., 2017). The value of η is 1 and 2 in lower and higher voltage region for an ideal diode (Javaid et al., 2016). The higher estimated value of η for homojunction diodes substantiates non linearity and the reason is attributed to present defects at the junction which is very common in solution processed devices exhibiting the presence of interfacial defects, presence of parasitic rectifying junctions, deep level defects assisted tunneling, and presence of electron-hole recombination in the depletion region(Lu et al., 2006; Vabbina et al., 2017).

We have estimated saturation current Is by using the formula

$I_s = A^* A T^2 [\exp(-q\varphi_B / k_B T)]$ (5.2)

where A^* is Richardson constant ($A^* = 32 A/cm^2K^2$ for ZnO), A represents effective are of the electrode and φ_B is barrier height at the junction (Somvanshi and Jit, 2014).

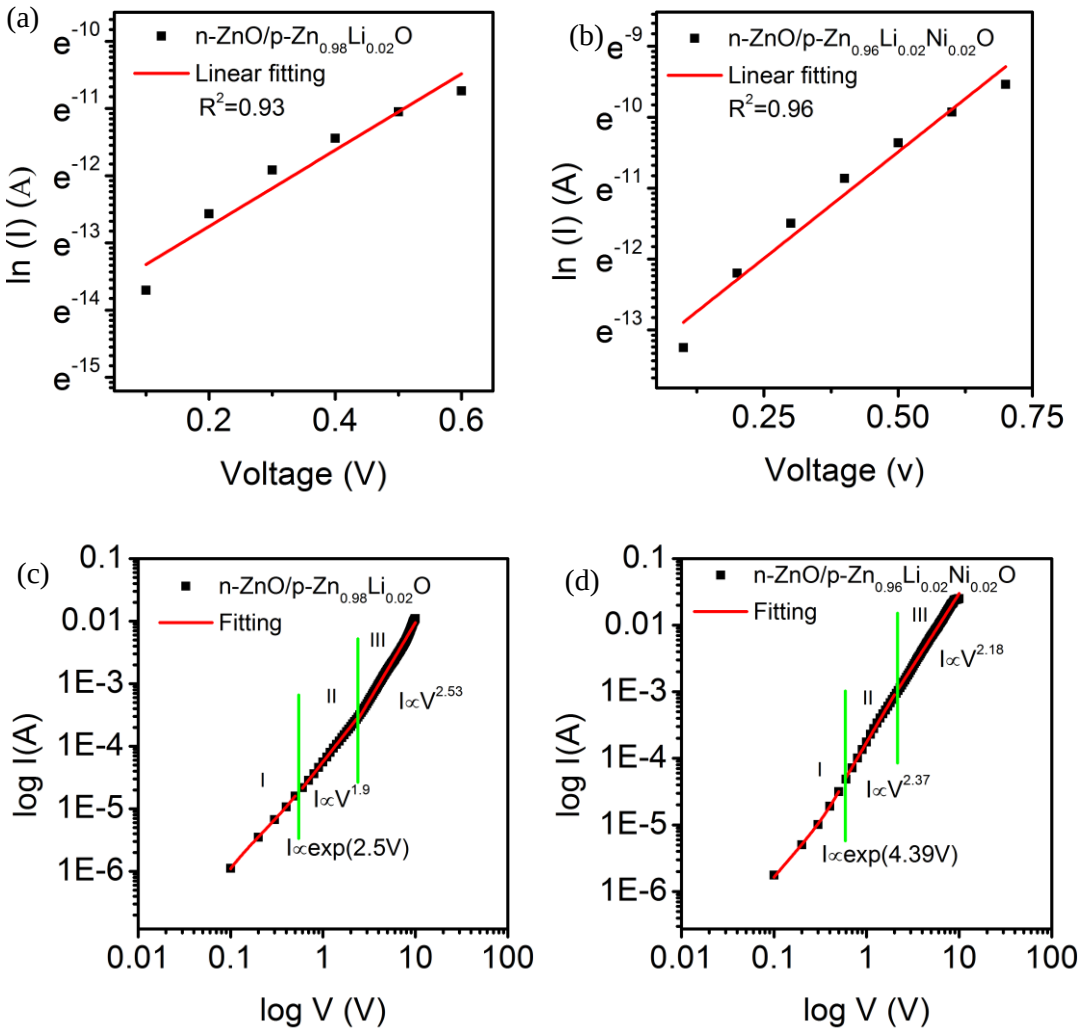

Figure 5.6 : (a) Linear fitted semilogrithim graph of n-ZnO/p- $Zn_{0.98}Li_{0.02}O$ diode, (b) Linear fitted semilogrithim graph of n-ZnO/p- $Zn_{0.96}Li_{0.02}Ni_{0.02}O$, (c) Current conduction mechanism of n-ZnO/p- $Zn_{0.98}Li_{0.02}O$ and (d) n-ZnO/p- $Zn_{0.96}Li_{0.02}Ni_{0.02}O$ diodes in forward biased region

Another method, known as Cheung's model, is also used to calculate the value of η and Φ_B where series resistance is also taken into consideration (Cheung and Cheung, 1986). Cheung's model expresses I-V relation as $dV/d\ln(I) = (\eta k_B T/q) + IR_s$ and $H(I) = V - (\eta k_B T/q)\ln(I/AA^*T^2)$; where $H(I) = \eta \Phi_B + IR_s$ where, R_s represents series resistance. The estimated value of ideality factor and series resistance is relatively less for $Zn_{0.96}Li_{0.02}Ni_{0.02}O$ based homojunction, substantiating more ideal and conducting behaviour. The various estimated device parameters by both the models are given in Table 5.2.

Table 5.2 : Ideality Factor and Barrier Heights of The Diodes Using Thermionic Model and Cheung model(Somvanshi and Jit, 2014)(Cheung and Cheung, 1986)

Homojunction device	η	η (Cheung)	Φ_B (eV)	Φ_B(eV) (Cheung)	R_s(kΩ)
n-ZnO/p- $Zn_{0.98}Li_{0.02}O$	6.78	4.26	0.65	0.66	11.7(12)

n-ZnO/p- $Zn_{0.96}Li_{0.02}Ni_{0.02}O$	5.95	3.58	0.64	0.64	2.9(3.4)

The current conduction mechanism in the forward region of these homojunctions are estimated by plotting logarithmic I-V curves which are presented in Figures 5.6 (c) and 5.6 (d) for $Zn_{0.98}Li_{0.02}O$ and $Zn_{0.96}Li_{0.02}Ni_{0.02}O$ based homojunctions, respectively. These measurements suggest that at lower voltage a recombination tunneling current mechanism is dominant which follows I α exp(αV);where α is a constant and V is voltage (Ye et al., 2006). Here, the exponential rise in current with respect to the voltage is evident which is common for a wide band gap MOS (Ye et al., 2006). The reason for this conduction mechanism is attributed to interface defects present at the junctions which prefers tunnelling over injection for recombination in the depletion region (Z. Shi et al., 2016). The power law $I \alpha V^m$ is observed in second and third voltage regions, where m is power exponent. m > 1 is observed in those voltage regions for homojunctions which supports space charge limited conduction (SCLC) mechanism for carrier transport at the junctions (Ye et al., 2006). The prefect diodes have m=2 but the observed diode in our case is non-linear due to effects of various defects which affect the conductions mechanism.

Further, to make sure that bottom silicon substrate is not participating in the diode behaviour of proposed work, we have synthesized p-ZnO/n-ZnO junctions on FTO coated glass substrate. The SEM analysis of the top view of junctions' ensures the formation of nanorods however the observed diameters of nanorods have been reduced (~100 nm) in comparison to silicon based devices. This change might be due to effect of substrate on the growth of nanorods which has been reported previously.

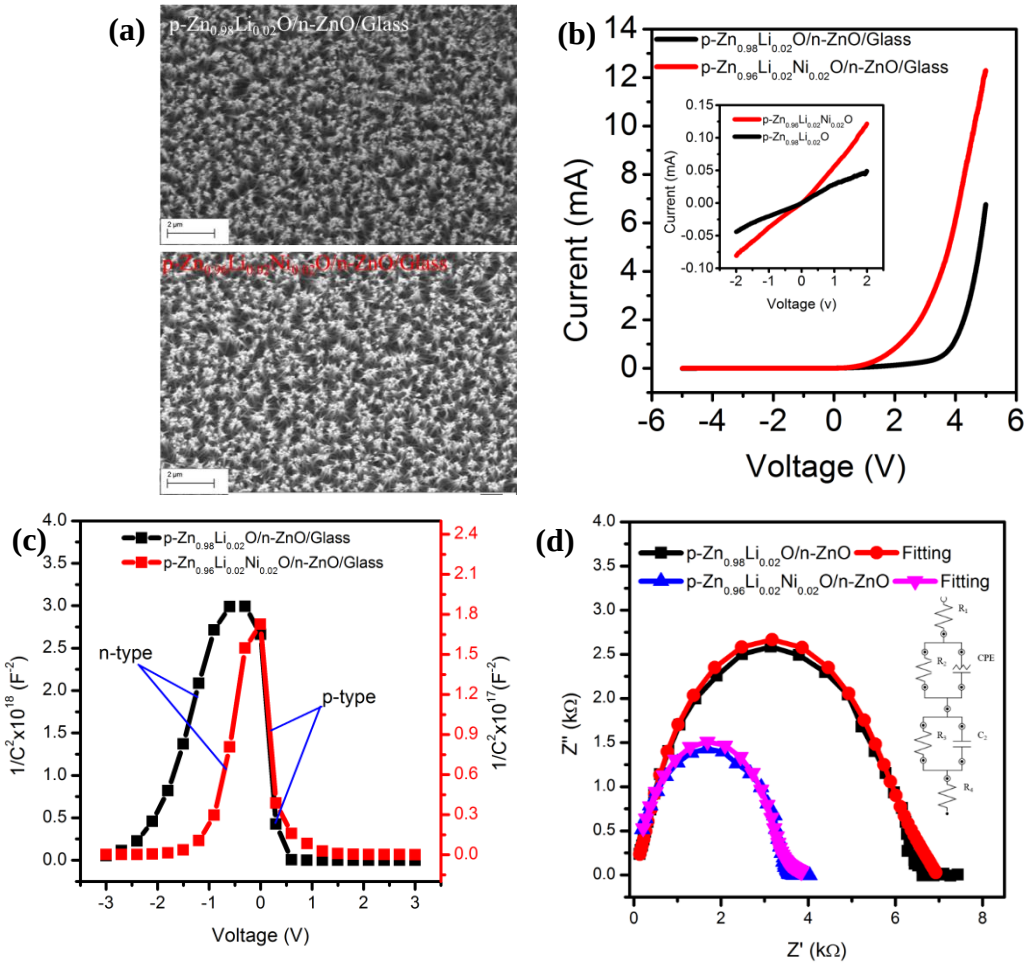

Figure 5.7: (a) Top view of SEM images of p-$Zn_{0.98}Li_{0.02}O$/n-ZnO and p-$Zn_{0.96}Li_{0.02}Ni_{0.02}O$/n-ZnO homojunctions (b) I-V graph of p-$Zn_{0.98}Li_{0.02}O$/n-ZnO and p-$Zn_{0.96}Li_{0.02}Ni_{0.02}O$/n-ZnO homojunctions with inset showing top p-p I-V characteristics (c) Mott-Schottky analysis of p-$Zn_{0.98}Li_{0.02}O$/n-ZnO and

p-$Zn_{0.96}Li_{0.02}Ni_{0.02}O$/n-ZnO p-n junctions showing inverted V shape (d) Electrochemical impedance spectra of p-$Zn_{0.98}Li_{0.02}O$/n-ZnO/Glass and p-$Zn_{0.96}Li_{0.02}Ni_{0.02}O$/n-ZnO/Glass homojunctions with electrochemically fitted circuit in the inset

The I-V analysis of top p-p contact showed ohmic behaviour, eliminating the effect of silver contact on the diode behaviour. The top and bottom configuration of I-V characteristics showed diode characteristics. The observed turn on voltage and on/off ratio for p-$Zn_{0.98}Li_{0.02}O$/n-ZnO (p-$Zn_{0.96}Li_{0.02}Ni_{0.02}O$/n-ZnO) is 4.2 V (3 V) and 80 (233), respectively. The change in values of these parameters might be attributed to change in nanorods diameter which changes the junction properties. Mott-Schottky analysis of the junctions showed inverted V type characteristic which signifies the presence of n and p-type ZnO. The positive slope represents n-type and negative slop represents p-type conductivity of the junctions. Further, we did impedance analysis on both the samples and the electrochemical circuit fit substantiates the presence of two type of layer in both the junctions. The fitted circuit is represented in the inset of figure 5.7 (d). Top and bottom contact resistances are represented by R1 and R4. p-ZnO layer is indicated by Parallel combination of R2 and CPE and n-ZnO by parallel combination of R_3 and C2. For p-$Zn_{0.98}Li_{0.02}O$/n-ZnO homojunctions, the calculated values of R_2, R_3 and C_2 are 4.4 kΩ, 2.62 kΩ and 1.41 nF, respectively. The estimated numbers of R_2, R_3 and C_2 for p-$Zn_{0.96}Li_{0.02}Ni_{0.02}O$/n-ZnO based devices are 2.7 kΩ, 2.68 kΩ and 0.8 nF, respectively. The estimated added resistance value R_1 and R_4 are equivalent for both the junctions which is ~500Ω. The values of n-ZnO for both the junctions are similar however the value of p-ZnO has changed significantly. Here, p-$Zn_{0.96}Li_{0.02}Ni_{0.02}O$/n-ZnO device have lower resistance whichis in accordance with the I-V results. Hence, substitution of nickel along with lithium is increasing the solubility of lithium acceptors in p-$Zn_{0.96}Li_{0.02}Ni_{0.02}O$/n-ZnO, resulting in improved rectification behaviour.

5. 4 Conclusions

We have optimized the synthesis process for n-ZnO, p- $Zn_{0.98}Li_{0.02}O$ and p-$Zn_{0.96}Li_{0.02}Ni_{0.02}O$ type uniformly distributed and highly oriented nanorods. Further, we synthesized two different homojunctions using these p-type ZnO with n-ZnO nanorods. The XRD analysis substantiates the uniform incorporation of acceptor atoms with preferred (002) orientation. The surface images of samples showed the formation vertically aligned nanorods with diameters ~ 120 nm. The corss-sectional SEM analysis confirmed the synthesis of nanorods based p-n junction. The Mott-Schottky analysis substantiates relatively higher acceptor concentration in p- $Zn_{0.96}Li_{0.02}Ni_{0.02}O$ nanorods. $Zn_{0.96}Li_{0.02}Ni_{0.02}O$ homojunction showed lower turn on voltage with higher rectification in comparison to $Zn_{0.98}Li_{0.02}O$ based homojunction diode. Lower values of ideality factor and barrier height are observed for n-ZnO/p-$Zn_{0.96}Li_{0.02}Ni_{0.02}O$ homojunctions in comparison to n-ZnO/p- $Zn_{0.98}Li_{0.02}O$ diodes. The current conduction mechanism in both the homojunctions is attributed to tunnelling in lower voltage region and SCLC in higher voltage region.